estec

European Space Research
and Technology Centre
Keplerlaan 1
2200 AG Noordwijk
The Netherlands
Tel. +31 71 565 8332
www.esa.int

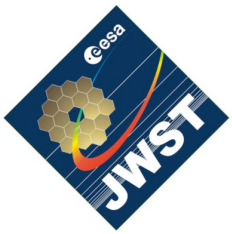

NIRSpec Technical Note
NTN-2013-009

Authors: Guido De Marchi & Torsten Böker

Date of Issue: 9 November 2013
Version: 1

Observations acquired during NIRSpec's ground calibration to validate the on-board scripts for target acquisition

ABSTRACT

This note describes the observations collected during the second NIRSpec ground calibration campaign in order to validate the effectiveness of the on-board scripts for target acquisition.

1 INTRODUCTION

During the second NIRSpec ground calibration campaign, conducted in 2013 January and February (Gnata et al. 2013), a series of exposures were collected to test and validate the automated target acquisition scripts that will run on board NIRSpec once in orbit. The NIRSpec target acquisition concept is presented and extensively described in Jakobsen (2004a, 2004b, 2005) and the necessary requirements are listed in Böker (2008). We assume that the reader is familiar with the target acquisition process, but we recall here that the purpose of the NIRSpec target acquisition software is to autonomously calculate and then apply the spacecraft slew needed to align the micro-shutter array (MSA) with a set of target sources in the sky.

As part of the target acquisition process, two exposures are collected of a set of reference stars through the all-open MSA in imaging mode. The two exposures are separated by a spacecraft slew corresponding to half the micro-shutter pitch (about 120 mas in X and 250 mas in Y). This "half MSA facet slew" is necessary to properly derive the location of the reference stars, taking into account the presence of the physical bars between micro-shutters that could otherwise bias the measured positions of the stars. Both images are processed by the on-board software, first to correct for pixel-to-pixel response variations and finally to determine the precise locations of the reference stars. These locations are initially measured in pixel coordinates and must be transformed by the software into the distortion-free, tangential coordinate system on the sky, before they can be compared to the desired "ideal" positions. This coordinate transformation requires precise knowledge of the combined distortion effects of telescope (optical telescope element or OTE) and NIRSpec, as well as the measured tilt of the imaging mirror. Finally, comparing the measured reference star positions on the sky with the "ideal" positions as specified by the observer during the

planning stage will allow the software to compute the final corrective spacecraft slew, and to communicate it to the attitude control system (ACS).

The exposures described here, collected during the second NIRSpec ground calibration campaign, follow the rationale of the verification plan put forth by Lambros & Ramey (2008). These exposures allow for the verification of some of the steps broadly described above, namely the precise determination of the position of the reference stars, in pixel coordinates. Once the images and ancillary telemetry information generated by NIRSpec using the optical ground support equipment are delivered to NASA, the remaining target acquisition process, up to the point of the generation of the small angle manoeuvre offset command, can be tested. Note that it will not be possible at this stage to translate the coordinates of the reference stars to the plane of the sky, since no telescope optics were present during the calibration tests. However, it is possible to translate those positions to the image plane at the entrance of NIRSpec (i.e. at the OTEIP), and accurate geometric transformations between the relevant image planes (i.e. between the OTEIP and MSA and between the MSA and detectors and viceversa) are now available. Therefore, the exposures described here will permit a realistic verification of the autonomous target acquisition scripts.

The remainder of this note provides a brief description of the instrumentation setup and some known limitations (Section 2), and describes the observations and the structure of the data files (Section 3). Finally, Section 4 describes some open issues with the coordinate transformations that will need to be addressed before a full end-to-end test of the on-board TA process is possible.

2 OBSERVATIONAL SETUP

The measurements described in this report were acquired during the second NIRSpec ground calibration campaign conducted by ESA and Astrium at the Industrieanlagen-Betriebgesellschaft (IABG) facility in Ottobrunn, Germany (Gnata & Candeias 2013). A high-level description of the optical ground support equipment (OGSE) used for these tests is contained in Birkmann (2011a). For the observations described here, the most relevant components inside the main chamber are the cryo-mechanism (CMO) with its dedicated pinhole mask (PHM) and the continuum source (0.6–5.0 μm) for pinhole mask imaging (PSB).

The PHM is located at the entrance plane of NIRSpec and the regularly spaced pinholes cover the entire extent of the MSA quadrants, with up to 121 (11×11) pinholes included in the field of view of each quadrant, depending on the actual position of the PHM. The knowledge of the pinhole absolute position with respect to the reference frame is better than 0.01 mm and the knowledge of the position of one pinhole relative to another is better than 0.001 mm. These uncertainties must be taken into account when the PHM is moved to simulate the half MSA facet offset, but they are very small and will not introduce systematic effects in the measurements.

The pitch of the micro-shutters is 0.105 mm in the X (or dispersion) direction and 0.204 mm in the Y (or spatial) direction. The scale factor between the PHM and the MSA plane is 0.614 in X and 0.605 in Y and, therefore, a half MSA facet offset will require a displacement of the PHM of 0.086 mm in X and 0.169 mm in Y. The detailed offsets applied between exposures with the same

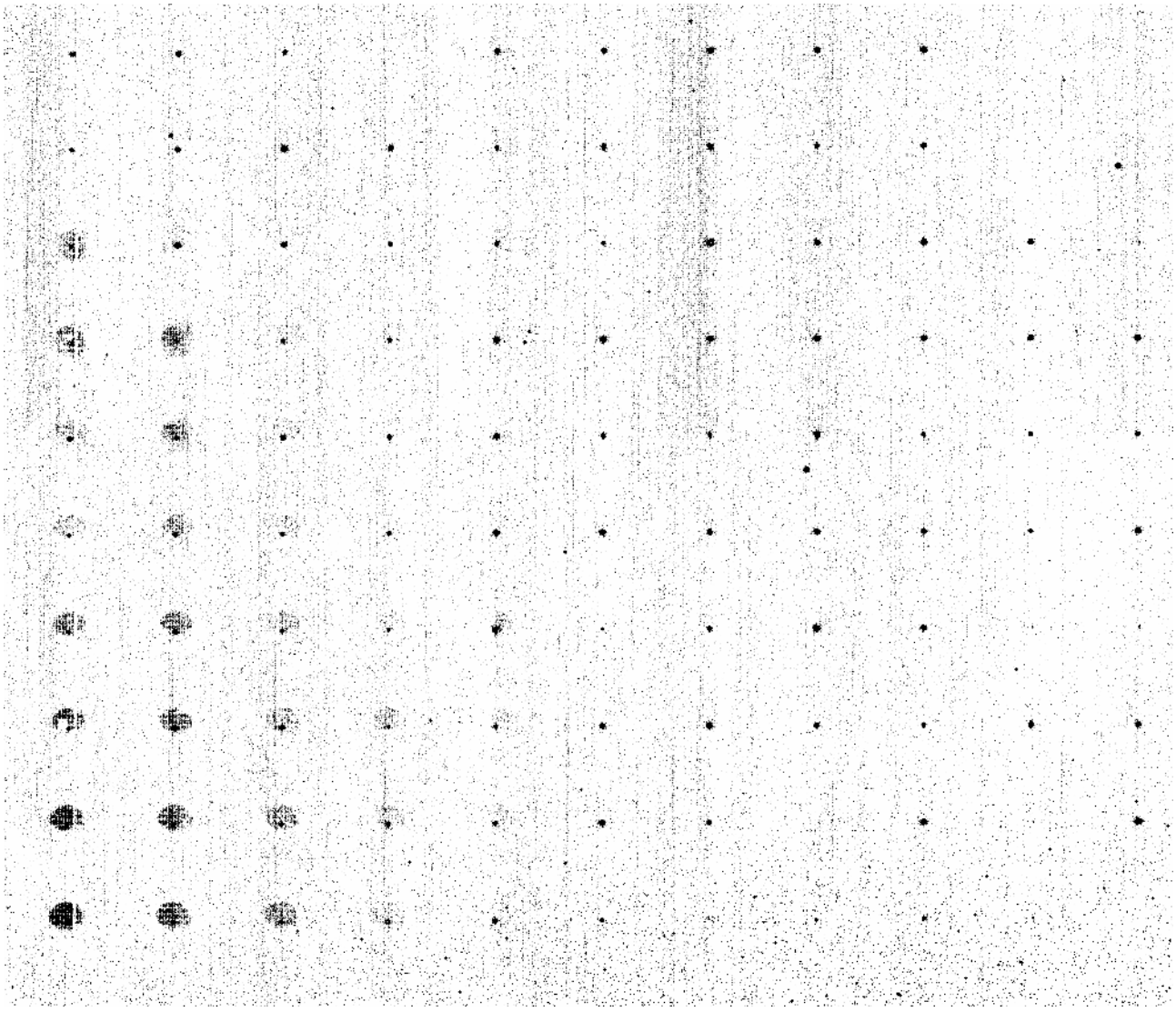

Figure 1. Negative image showing the pinholes as imaged though quadrant Q4 of the MSA. Due to the uneven size of the holes in the PHM, not all pinhole images have the same size or intensity.

configuration are discussed in Section 3.

The average pinhole diameter is 8.0 μm with a standard deviation (1 sigma) of 1.3 μm. Therefore, some of the pinholes are too small to produce point-like images bright enough to achieve a SNR of at least 20 at the peak (Jakobsen 2004a) in exposures lasting three groups. On the other hand, since there are typically more than 100 pinholes visible through each MSA quadrant, there are enough sources to simulate sufficiently bright reference stars in all exposures. As an example, the detector region containing the pinholes as seen through quadrant Q4 is shown in Figure 1.

Note that in some cases, a halo is seen around the pinhole images, particularly those seen through

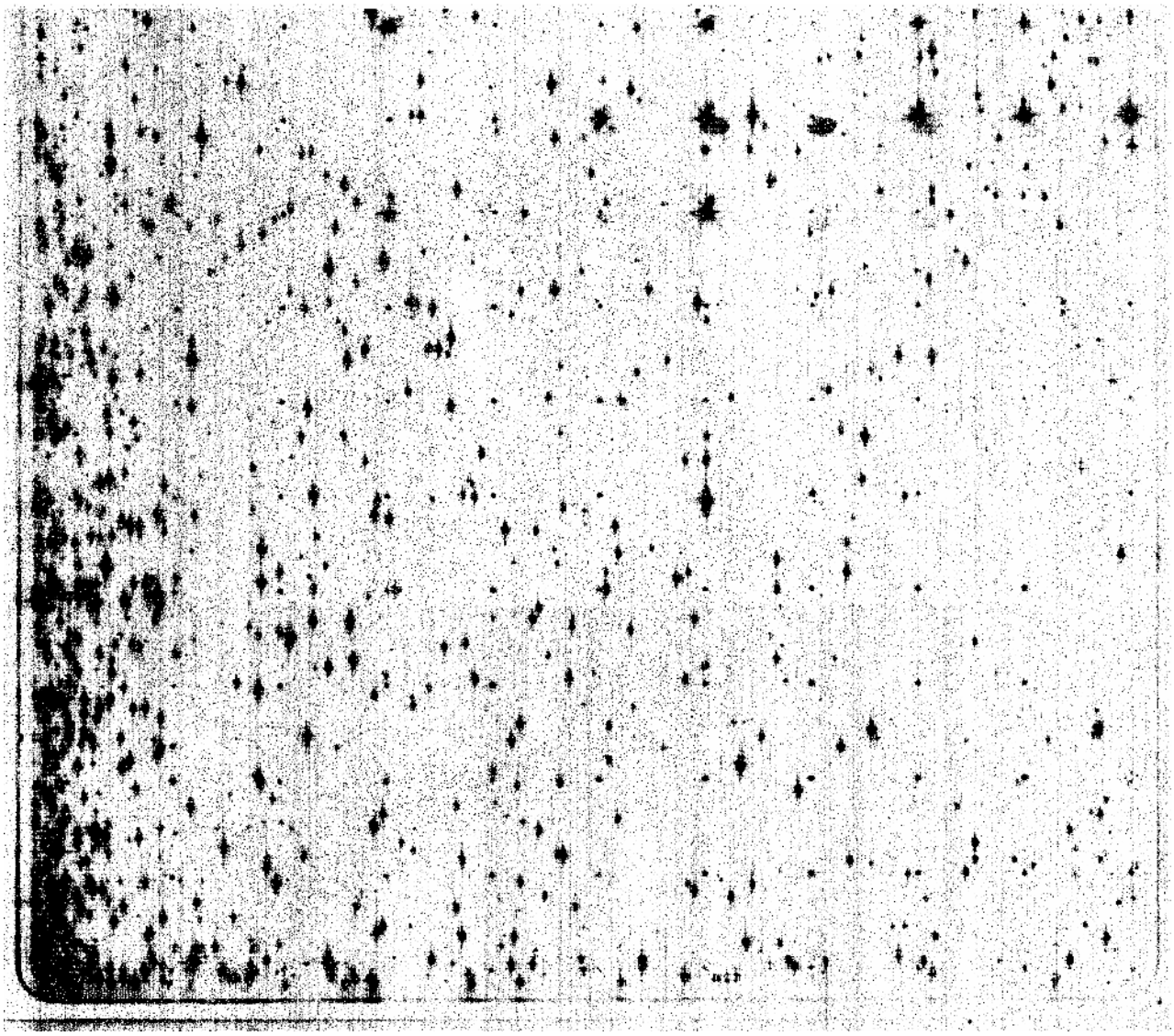

Figure 2. When the MSA magnet arm is kept at its secondary park position (LATCHUP), the higher than normal voltage used results in significant glowing of some shorted shutter. The effect is particularly severe in quadrant Q3. The region of the detector corresponding to this quadrant is also affected by a large number of hot pixels.

the top right portion of quadrant Q1 and the bottom left portion of quadrant Q4 (see Figure 1). The haloes are purely an OGSE-related effect. In order to ensure a high enough flux through the pinholes, the most powerful light source available (PSB) is used. Since the pinhole mask has a total hemisphere reflectivity of about 10%, the use with the PSB induces a very large amount of background light in the chamber. This parasitic light finds its way to the other side of the PHM and is therefore detected by NIRSpec. This straylight, however, has no significant impact on the accuracy of the computation of the centroid of the PSF associated with the pinholes.

Although pinholes can be identified and their positions measured across the whole MSA field of view, there are two reasons making the use of pinholes falling on quadrant Q3 more problematic. One is an unwelcome effect in the observational setup causing a light “glow” associated to some

micro-shutters. The problem is due to shorts in the substrate and is particularly severe only for quadrant Q3 (see Figure 2). After the problem was discovered, the MSA team were able to implement a workaround in which only one hold voltage is used instead of two (columns and rows) to command the shutters. This has drastically reduced the leakage current at shutter level and therefore the glow has disappeared. However, as explained in Section 3, some of the observations to verify the target acquisition scripts were acquired with the MSA magnet arm in its secondary park position (also called LATCHUP), in which no such workaround is possible. Hence, those exposures are affected by significant glow in quadrant Q3, where glowing shorts appear as bright sources, effectively brighter than the pinholes, as shown in Figure 2. In principle, pinholes located in regions of quadrant Q3 not affected by glowing shorts could be used to validate the target acquisition procedure, but since there are enough pinholes in the regions corresponding to the other three quadrants, not affected by glowing shorts, this will not be necessary. This problem is only present in the first set of observations, while the remaining four are free from glowing shorts (see Section 3).

The other reason to exclude from the tests the regions corresponding to quadrant Q3 is the large amount of hot pixels present in those parts of the detector (number 491, see Sirianni 2013). Due to a degradation caused by a design flaw in the barrier layer of the pixel interconnect structure, the detectors currently installed in NIRSpec have been declared non-flight worthy and will be replaced before launch. The situation is particularly acute in the region corresponding to quadrant Q3 (see Figure 2), where severe degradation and increase in the number of hot and warm pixels has been witnessed between the first and second ground calibration campaigns of NIRSpec, conducted two years apart. The number of hot pixels (defined as those with a dark current of 0.1 electron/s or more) has increased by a factor of ~2.5 reaching almost 8% of the total surface of the detector (and more in the specific area corresponding to quadrant Q3). The number of "warm" pixels, defined as those with dark current between 0.01 and 0.1 e-/s, has also doubled. Considering that such a large number of hot pixels is not representative of the detectors with which NIRSpec will be equipped when in flight, tests of the onboard scripts conducted with those data might not provide realistic answers. Since, as noted above, there are enough pinholes in the regions corresponding to the other three quadrants, not affected so badly by hot pixels, it is advisable to restrict the validation of the tests to those regions.

3 OBSERVATIONS

The exposures needed to verify the target acquisition scripts were acquired as part of the procedure IMA-TA, in which the PSB source is used to illuminate the PHM. Five pairs of identical exposures were taken, each pair consisting of two exposures shifted by half a MSA facet, both in dispersion and spatial directions, whereas the five pairs are shifted with respect to each other by a known amount, ranging typically from 1" to 2". The exposures and the corresponding OGSE parameters are listed in Table 1 and briefly described below.

The test begins with an internal calibration exposure, namely an image of the flatfield source (called TEST) in the internal calibration assembly through the fixed-slits with the MSA in all closed position. This image could in principle serve for the calibration of the tilt angle of the grating wheel mirror, although we have demonstrated (De Marchi 2012; De Marchi et al. 2012; Alves & De Marchi 2013) that this will in all likelihood not be necessary in orbit, since we can trust the tilt sensor installed on the grating wheel. We have decided to take this exposure nonetheless, should we encounter any problem with the sensors.

NID (1)	OBS_ID (2)	DATE (3)	GWA_XTIL (4)	GWA_YTIL (5)	CAA_LAMP (6)	FWA_POS (7)	CLS_CONF (8)	CMO_PHMX (9)	CMO_PHMY (10)	MSA_CONF (11)
8537	IMA-TA-001	2013-01-15T01:22:10	0.33947131	0.19679530	TEST	OPAQUE	CLOSE	0.000000	0.000000	CLOSED
8538	IMA-TA-002	2013-01-15T01:28:29	0.33947131	0.19679530	NO_LAMP	F110W	PSB	0.000000	0.000000	LATCHUP
8539	IMA-TA-003	2013-01-15T01:33:26	0.33947131	0.19679530	NO_LAMP	F140X	PSB	0.000000	0.000000	LATCHUP
8540	IMA-TA-004	2013-01-15T01:37:11	0.33947131	0.19679530	NO_LAMP	F140X	PSB	0.085503	0.168596	LATCHUP
8541	IMA-TA-005	2013-01-15T01:44:33	0.33947131	0.19679530	NO_LAMP	F110W	PSB	0.085503	0.168596	LATCHUP
8542	IMA-TA-006	2013-01-15T01:51:07	0.33999377	0.19680730	TEST	OPAQUE	CLOSE	0.342008	1.011577	IFUOPEN
8543	IMA-TA-007	2013-01-15T01:58:05	0.33999377	0.19680730	NO_LAMP	F110W	PSB	0.342008	1.011577	IFUOPEN
8544	IMA-TA-008	2013-01-15T02:01:22	0.33999377	0.19680730	NO_LAMP	F140X	PSB	0.342008	1.011577	IFUOPEN
8545	IMA-TA-009	2013-01-15T02:05:54	0.33999377	0.19680730	NO_LAMP	F140X	PSB	0.256506	1.180174	IFUOPEN
8546	IMA-TA-010	2013-01-15T02:13:11	0.33999377	0.19680730	NO_LAMP	F110W	PSB	0.256506	1.180174	IFUOPEN
8547	IMA-TA-011	2013-01-15T02:18:42	0.33926606	0.19677249	TEST	OPAQUE	CLOSE	-0.513013	0.674385	IFUOPEN
8548	IMA-TA-012	2013-01-15T02:25:41	0.33926606	0.19677249	NO_LAMP	F110W	PSB	-0.513013	0.674385	IFUOPEN
8549	IMA-TA-013	2013-01-15T02:29:38	0.33926606	0.19677249	NO_LAMP	F140X	PSB	-0.513013	0.674385	IFUOPEN
8550	IMA-TA-014	2013-01-15T02:32:43	0.33926606	0.19677249	NO_LAMP	F140X	PSB	-0.598514	0.505788	IFUOPEN
8551	IMA-TA-015	2013-01-15T02:39:40	0.33926606	0.19677249	NO_LAMP	F110W	PSB	-0.598514	0.505788	IFUOPEN
8552	IMA-TA-016	2013-01-15T02:46:23	0.34122738	0.19681810	TEST	OPAQUE	CLOSE	-0.342009	-0.674385	IFUOPEN
8553	IMA-TA-017	2013-01-15T02:53:38	0.34122738	0.19681810	NO_LAMP	F110W	PSB	-0.342009	-0.674385	IFUOPEN
8554	IMA-TA-018	2013-01-15T02:57:23	0.34122738	0.19681810	NO_LAMP	F140X	PSB	-0.342009	-0.674385	IFUOPEN
8555	IMA-TA-019	2013-01-15T03:00:29	0.34122738	0.19681810	NO_LAMP	F140X	PSB	-0.256506	-0.842981	IFUOPEN
8556	IMA-TA-020	2013-01-15T03:07:26	0.34122738	0.19681810	NO_LAMP	F110W	PSB	-0.256506	-0.842981	IFUOPEN
8557	IMA-TA-021	2013-01-15T03:18:07	0.33988181	0.19684091	NO_LAMP	F110W	PSB	0.513013	-1.011577	IFUOPEN
8558	IMA-TA-022	2013-01-15T03:21:25	0.33988181	0.19684091	NO_LAMP	F140X	PSB	0.513013	-1.011577	IFUOPEN
8559	IMA-TA-023	2013-01-15T03:25:10	0.33988181	0.19684091	NO_LAMP	F140X	PSB	0.598515	-0.842981	IFUOPEN
8560	IMA-TA-024	2013-01-15T03:31:57	0.33988181	0.19684091	NO_LAMP	F110W	PSB	0.598515	-0.842981	IFUOPEN
8561	IMA-TA-025	2013-01-15T03:38:40	0.33988181	0.19684091	TEST	OPAQUE	CLOSE	0.513013	-1.011577	CLOSED

Table 1. List of the observations collected during the NIRSpec ground calibration campaign to validate the on-board target acquisition scripts. The columns are as follows: (1) observation ID (1), (2) name and number of the procedure, (3) date, (4) reading of the XTIL telemetry sensor in dispersion direction, (5) reading of the XTIL telemetry sensor in cross-dispersion direction, (6) name of the internal calibration lamp used, (7) name of the filter, (8) name of the external calibration lamp used, (9) position of the PHM in the X direction in mm, (10) position of the PHM in the Y direction in mm, (11) name of the MSA configuration.

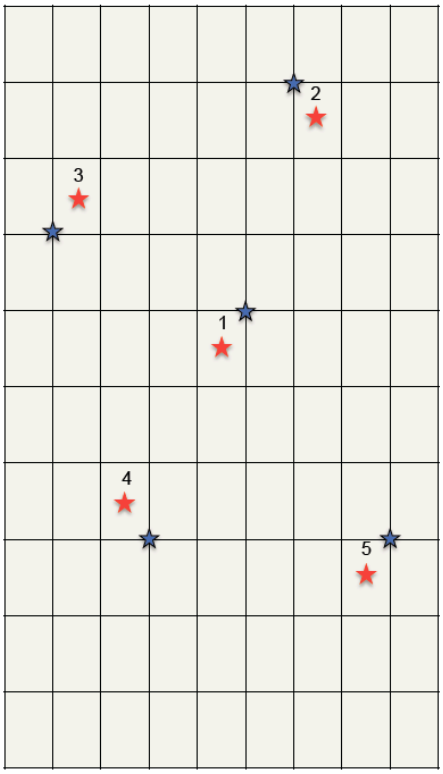

Figure 3. Schematic view of the half MSA facet offsets commanded during the observations between the first (red) and second (blue) exposure in each pair.

The test then continues by producing the first exposure of the pair (actually two since both target acquisition filters F110W and F140X are used). The sequence is as follows: reconfigure the MSA in an all open pattern; place the pinhole mask in a known position; configure the calibration light source (CLS) to select the PSB source; take an exposure through each of the two target acquisition filters. The second exposures set of the pair is generated in the same way, but after the PHM has been translated in such a way that the point sources are shifted in the OTE image plane by an amount that corresponds to half a MSA facet both in the dispersion and spatial directions. Information on both the starting and ending positions of the pinhole mask are stored in the telemetry and in the fits header (keywords `CMO_PHMX, CMO_PHMY`) and provided in Table 1.

The entire procedure is then repeated four more times, in order to produce five independent pairs of simulated target acquisition images with a matching fixed-slit image to verify the position of the grating wheel mirror, since the latter is cycled in between exposure pairs. These pairs are typically shifted by 1” to 2” from the initial set, in random directions not parallel to the MSA axes. These offsets are sufficiently small to guarantee a high accuracy of the relative positions of the pinhole mask. All four possible directions of the half-facet offsets are used, as shown schematically in Figure 3 (the offsets shown are for illustration purposes only). The relative offsets between the different positions of the PHM are shown in Table 1 by the corresponding movements (in mm) of the cryo mechanism, and are also summarised in Table 2 in units of one MSA shutter, with respect to the starting position (0, 0).

Pair	Position A	Position B
1	(0.0, 0.0)	(+0.5, +0.5)
2	(+2.0, +3.0)	(+1.5, +3.5)
3	(-3.0, +2.0)	(-3.5, +1.5)
4	(-2.0, -2.0)	(-1.5, -2.5)
5	(+3.0, -3.0)	(+3.5, -2.5)

Table 2. Shifts applied to the PHM masks during the test, expressed in units of one MSA microshutter. Position A and B refer, respectively, to the positions before and after the commanded half-facet offset.

During this procedure the MSA was commanded in a fashion similar to that planned for in-orbit target acquisition, to verify that the planned approach is valid. In the target acquisition scenario, one possibility that has been discussed is that the MSA magnet arm is moved to its secondary park position (LATCHUP) and kept there during the exposures of the reference stars. In this case, only once the centroids of the reference stars are determined is the MSA reconfigured as needed for the science observations. In other words, this approach only uses one full MSA cycle (i.e. one sweep "up" and one sweep "down"), rather than using two if the MSA were first commanded to a fully open configuration and then again to the desired configuration. During these tests, we have used both approaches, i.e. the one using a LATCHUP and the one using a fully open configuration (IFUOPEN). This will allow us to check for possible differences. This is particularly true in the case of the images of the fixed slits, used to determine the actual orientation of the grating wheel, which have been taken with the MSA in IFUOPEN, CLOSED and LATCHUP configurations.

The exposure times used for the observations are meant to reach a signal-to-noise ratio of about 20 on average in the peak of well exposed, unobstructed pinholes in exposures with `NGROUP`=3. However, lower or higher values are possible because of the different sizes of the pinholes, as mentioned in Section 2. All exposures through the F110W filter have NGROUP=20, while those through F140X are of shorter duration (NGROUP=10), since this filter is considerably wider than F110W. Note that due to the limitations of the data storage units (SCEPs) used for on-board data processing, only three frames can be processed in orbit. These three frames will be used to remove detector bias and cosmic rays before centroiding via pairwise differencing. The fact that the on-ground exposures discussed here are longer provides an opportunity to simulate data with different signal-to-noise ratios by selecting frames with varying intervals between them. For example, selecting frames 8, 9, and 10 to calculate the differences (9-8) and (10-9) will yield an effective exposure time of 10.76 s (i.e. one frame time) while using frames 2, 6, and 10 will yield a four times longer effective exposure time.

The observations are stored in fits files organised in directories, called after the procedure name (`OBS_ID`) and date, as per columns 2 and 3 in Table 1. Each directory contains, amongst others, the raw fits files and the pre-processed count-rate fits files (Birkmann 2011b) for both NIRSpec detectors (respectively marked with the code names 491 and 492). The files are accessible via anonymous FTP on the server `ftp.rssd.esa.int` in the directory `pub/jwstlib/TargetAcq` or with a web browser by visiting the link `ftp://ftp.rssd.esa.int/pub/jwstlib/TargetAcq`.

In order to facilitate the identification of the pinhole images in these exposures, we also provide tables (in ASCII format) with the coordinates of the pinholes in detector reference system, for some of the exposures. More precisely, we provide these lists for all the observations taken through the F140X filter, for each of the PHM positions. The pinhole positions for the observations obtained

through the F110W filter, for the same PHM positions, only differ by a fraction of a pixel from those for the F140X filter. Thus, it is safe to use the latter in order to define the 32×32 pixel^2 regions that the on-board script will use for centroiding. The files are named "`pinholes_####.txt`", where `####` is the ID of the exposure (`NID` in Table 1) and are located in the directory corresponding to that exposure. Each file contains four columns: the first is the detector ID (1 or 2, respectively for detectors 491 and 492), the second and third columns provide the X and Y coordinates of the pinholes in the detector reference frame, while the fourth column gives the amplitude of the pinhole image in units of count/s. All coordinates are given in the reference frame as defined by the FITSWRITER routine, starting from (1,1).

4 COORDINATE TRANSFORMATIONS

As mentioned in the Introduction, a complete verification of the target acquisition scripts requires the use of coordinate transformations between the relevant optical planes, namely between the FPA and the MSA and between the MSA and the sky. The first of these transformations must account for the distortions introduced by the collimator optics and by the camera optics. Furthermore, this transformation also depends on the actual position of the imaging mirror installed on the grating wheel assembly (GWA).

The mechanical angular reproducibility of the GWA mechanism is typically very good, thanks to the very high quality bearings and ratchet assembly, and a reproducibility of ~2.5 arcsec (1 σ) is normally achieved (Weidlich et al. 2008; Leikert 2008). However, for optimal scientific performance this is not sufficient, as even this small angular variation already changes the position of the image on the detector plane by ~0.4 pixel. To overcome these limitations, a grating wheel tilt sensor system has been developed and installed on NIRSpec and we have shown that these magneto-resistive position sensors provide very accurate information on the position of the wheel and of the actual orientation of the selected GWA optical element (De Marchi 2012; De Marchi et al. 2012; Alves & De Marchi 2013). We have also shown that a linear relationship can in general be defined between the readings of the GWA tilt sensor and the pixel offsets on the detector (De Marchi & Giardino 2013). On the other hand, although the residuals are small (less than 2.5 mas RMS), they are not independent of the offsets themselves. More precisely, a GWA tilt does not result in a simple "bulk" shift across the detectors, and residuals of order ±1.5 % of the average shift are found, depending on the field angle (De Marchi & Giardino, in preparation). This is due to the fact that a GWA tilt causes the same feature in the MSA plane to be seen under a slightly different angle from the detector, which results in a different set of coefficients for the coordinate transformation due to the optical distortion intrinsic to the camera optics. For an offset of up to 2 pixel, as observed during the second NIRSpec ground calibration campaign, this implies a variation of about 0.02 pixel or 2 mas across the field of view.

The correct treatment of the grating wheel tilt requires a two-step approach. First, the centroid positions on the FPA (in pixel space) must be converted to the GWA plane (in angular coordinates), and the correction for the actual GWA tilt angle (derived from the sensor telemetry) is applied in these angular coordinate system. In a second step, the GWA coordinates are transferred to the MSA plane, and then to the OTEIP/sky.

The NIRSpec parametric model (Giardino 2013) already includes separate transformations

between the detector plane and the GWA plane, and between the GWA plane and the MSA plane. The model can therefore accurately calculate the combined coordinate transformation between the detector and MSA planes, for each value of the GWA tilt. It is thus possible for the on-board target acquisition scripts to use a similar approach, i.e. a two-step coordinate transformation between FPA and MSA, with an intermittent tilt correction, to calculate the position of the references stars on the sky and to derive the corrective telescope slew for a successful target acquisition.

REFERENCES

Alves de Oliveira, C., De Marchi, G. 2013, "Calibration of the GWA position sensors – Part II," NPR-2013-008 / ESA-JWST-RP-19657 (Madrid: ESAC)

Birkmann, S. 2011a, "Description of the NIRSpec optical ground support equipment (OGSE)," ESA-JWST-TN-18255 (Noordwijk: ESTEC)

Birkmann, S. 2011b, "Description of the NIRSpec pre-processing pipeline," NTN-2011-004 (Noordwijk: ESTEC)

Böker, T. 2008, "Target Acquisition Requirements," ESA-JWST-RQ-5071 and JWST-RQMT-006993 (Noordwijk: ESTEC)

De Marchi, G. 2012, "Calibration of the GWA position sensors – Part I," NPR-2012-002 (Noordwijk: ESTEC)

De Marchi, G., Birkmann, S., Böker, T., Ferruit, P., Giardino, G., et al. 2012b, "Calibrating the position of images and spectra in the NIRSpec instrument for the James Webb Space Telescope," Proc. SPIE 8442-84423G

Giardino, G. 2013, "An introduction to the NIRSpec parametric model,'' NTN-2013-011 (Noordwijk: ESTEC)

Gnata, X., Candeias, H. 2013, "FM calibration and verification report," NIRS-ASD-TR-0143 (Ottobrunn: EADS)

Jakobsen, P. 2004a, "The NIRSpec Target Acquisition Concept," ESA-JWST-TN-650 (Noordwijk: ESTEC)

Jakobsen, P. 2004b, "NIRSpec Target Acquisition and the Micro Shutter Array," ESA-JWST-AN-1060 (Noordwijk: ESTEC)

Jakobsen, P. 2005, "Error Budget for NIRSpec Target Acquisition," ESA-JWST-AN-3032 (Noordwijk: ESTEC)

Lambros, S., Ramey, D. 2008, "Near Infrared Spectrograph Target Acquisition Verification Document ," JWST-PLAN-006511-DRAFT (Greenbelt: GSFC)

Leikert, T., 2011, "Alignment and testing of the NIRSpec filter and grating wheel assembly," Proc. SPIE 8131-25

Sirianni, M. 2013, "Status of the NIRSpec Focal Plane Array # 104 after the second (FM2) cyro campaign," ESA-JWST-RP-19658 (Noordwijk: ESTEC)

Weidlich, K., Fischer, M., Ellenrieder, M.M., Gross, T., Salvignol, J.C., et al. 2008, "High-precision cryogenic wheel mechanisms for the JWST NIRSpec instrument", Proc. SPIE 7018, 64